

Article

Receiving Paths Improvement of Digital Phased Array Antennas Using Adaptive Dynamic Range

Xuan Luong Nguyen ^{1,*} , Thanh Thuy Dang Thi ¹, Phung Bao Nguyen ² and Viet Hung Tran ²¹ Faculty of Physics, VNU University of Science, Ha Noi 100000, Vietnam; dangthithanhthuy@vnu.edu.vn² Department of Electronic Technology, Institute of System Integration, Le Quy Don Technical University, 236 Hoang Quoc Viet, Ha Noi 100000, Vietnam; nguyenphungbao@lqdtu.edu.vn (P.B.N.); hung.isi@lqdtu.edu.vn (V.H.T.)

* Correspondence: nguyenxuanluong_sdh22@hus.edu.vn

Abstract: In contemporary radar technology, the observation and detection of objects with low radar cross-sections remains a significant challenge. A multi-functional radar model employing a digital phased array antenna system offers notable advantages over traditional radar in addressing this issue. Nonetheless, to fully capitalize on these benefits, improving the structure of the receiving path in digital transceiver modules is crucial. A method for improving the digital receiving path model by implementing a matched filter approach is introduced. Given that the return signals from objects are often lower than the internal noise, the analog part of the digital transceiver modules must ensure that its dynamic range aligns with the level of this noise and the weak signal. The output signal level of the analog part must correspond to the allowable input range of the analog-to-digital converter. Improvements in the receiving path to achieve a fully matched model can reduce errors in the phase parameters and amplitudes of the useful signal at the output. The simulation results presented in this paper demonstrate a reduction in amplitude error by approximately 1 dB and a phase error exceeding 1.5 degrees for the desired signal at the output of each receiving path. Consequently, these improvements are expected to enhance the overall quality and efficiency of the spatial and temporal accumulation processes in the digital phased array antenna system. Furthermore, to maintain the matched filter model, we also propose incorporating an adaptive “pseudo-expansion” of the linear gain range. This involves adding a feedback stage with an automatic and adaptive bias voltage adjustment for the intermediate-frequency preamplifier in the analog part of the receiving path. Simulations to qualitatively verify the validity of this proposal are conducted using data from practical operational radar system models.

Keywords: radar cross-sections; digital transceiver modules; dynamic range; receiving path; analog (linear) part; digital part



Citation: Nguyen, X.L.; Dang Thi, T.T.; Nguyen, P.B.; Tran, V.H. Receiving Paths Improvement of Digital Phased Array Antennas Using Adaptive Dynamic Range. *Electronics* **2024**, *13*, 4161. <https://doi.org/10.3390/electronics13214161>

Academic Editor: Hristos T. Anastassiou

Received: 23 August 2024

Revised: 11 October 2024

Accepted: 22 October 2024

Published: 23 October 2024



Copyright: © 2024 by the authors. Licensee MDPI, Basel, Switzerland. This article is an open access article distributed under the terms and conditions of the Creative Commons Attribution (CC BY) license (<https://creativecommons.org/licenses/by/4.0/>).

1. Introduction

Today, significant emphasis is placed on the management and detection of objects characterized as “difficult to detect” through radar systems, garnering considerable interest not only within military contexts but also in civilian applications. Within radar theory, such entities are identified as possessing radar cross-section (RCS) values significantly below those of common objects [1–3]. In the radar equation, it is the only parameter that conveys information about the object to be detected [4–6].

In the field of radar engineering and technology, contemporary multi-functional radar systems are often characterized by the combination of a central processing system with a digital phased array antenna system (DPAA), which consists of digital transceiver modules (DTMs) arranged on the open side of the antenna. These DPAA systems offer significant advantages over traditional models in detecting objects with small RCSs, primarily due to their capability to generate a total multibeam digital antenna direction diagram of the

receiving paths ($D_{r,\Sigma}$), independent of the total direction diagram of the transmitting paths ($D_{t,\Sigma}$) [6–9]. The beams in the receiving direction diagram can vary in parameters such as width and spatial position of each beam, facilitating the spatial accumulation of very small return signals from objects with low RCSs. Nevertheless, the quality and the performance of the receiving path in the DTM significantly impact the aforementioned advantages of the DPAA [10,11]. Maintaining the integrity of characteristic parameters, particularly avoiding phase and amplitude errors in the output signals of the DTM, is crucial for enhancing the efficiency of signal accumulation and processing in subsequent stages. It should be acknowledged that a substantial body of research has been published on this issue [12–19]. In the majority of these studies, researchers have identified the necessity to expand the dynamic range (linear gain range) of the receiving paths and have provided detailed technical solutions to address this need [12–14]. In addition, some research results have proposed solutions that combine different methods to solve the challenge of detecting low-RCS objects, for example, expanding the dynamic range based only on increasing the dynamic range of a certain element (e.g., of the analog-to-digital converter (ADC)) in the receiving path [15,17–19], or increasing a receiver's overall linearity based on a digital nonlinear equalization (NLEQ) processor [14,16,18]. However, there is still an important issue: radio frequency (RF) receivers in general, and digital receivers and digital receiving paths in particular, often include components with different functions connected in series. According to classical signal filtering theory, these models are still often synthesized in the form of optimal filters to ensure the maximum signal-to-noise ratio at the output.

The primary objective of this paper is to propose an appropriate structural model for the receiving paths to address the challenge faced by multi-functional radar systems employing a DPAA integrated with a DTM (i.e., integrated with receiving paths) in detecting low-RCS objects. By conceptualizing the receiver, in general, and the receiving path, in particular, as a filter of the signal, this study evaluates and proposes improvements to the receiving path structure. This is accomplished by employing a fully matched filter model, which extends the linear range of the amplitude characteristic for the receiving path. These improvements are applied to the synthesis of the receiving path structure to enhance signal processing capabilities for detecting objects with low RCSs.

Based on the analysis illustrated by qualitative estimates, the second section of this paper examines the characteristics of the receiving path in DTMs when the input signal consists of return signals from objects with low RCSs. The third section presents the content related to improving the structure of the receiving path to reduce the amplitude and phase errors of the return signals. This increases the efficiency of their processing and contributes to ensuring the ability to observe and detect objects with low RCSs. A simulation summary and analytical commentary are presented in the fourth section. The conclusions are presented in the final section.

2. Characteristics of the Receiving Path in the DTMs of the DPAA

To elucidate the characteristics of the digital receiving path in the DTMs of the DPAA, we begin with the general model. In traditional radar systems, this is referred to as the digital receiver, whereas in radar systems employing a DPAA, it is known as the receiving path of DTMs. They both perform the function of receiving and filtering the return signals and converting them into digital data for further processing. Consequently, they both comprise two components, analog and digital, connected in series. Of these, the analog part is typically synthesized according to the superheterodyne model (Figure 1).

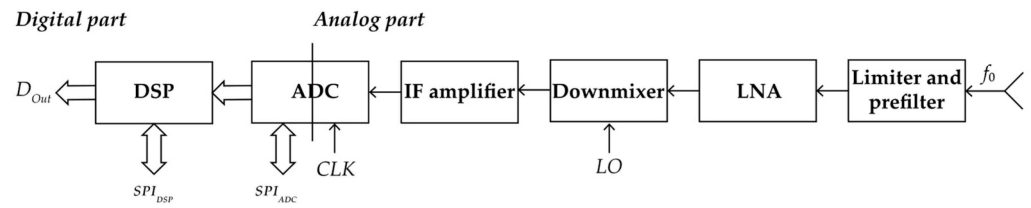


Figure 1. The general structure of the digital receiving model. f_0 —carrier frequency; LNA—low-noise amplifier; LO—local oscillator; CLK—clock controller signal; ADC—analogue-to-digital converter; SPI_{ADC} —serial peripheral interface of ADC; DSP—digital signal processor; SPI_{DSP} —serial peripheral interface of DSP; and D_{out} —digital signal at the output.

The first characteristic of the digital receiving path in DTMs for modern radars utilizing DPAA is its synthesis using the quadrature demodulation method, which employs two channels: in-phase (I) and quadrature (Q). Figure 2 illustrates the fundamental structure of the receiving path in the DTM.

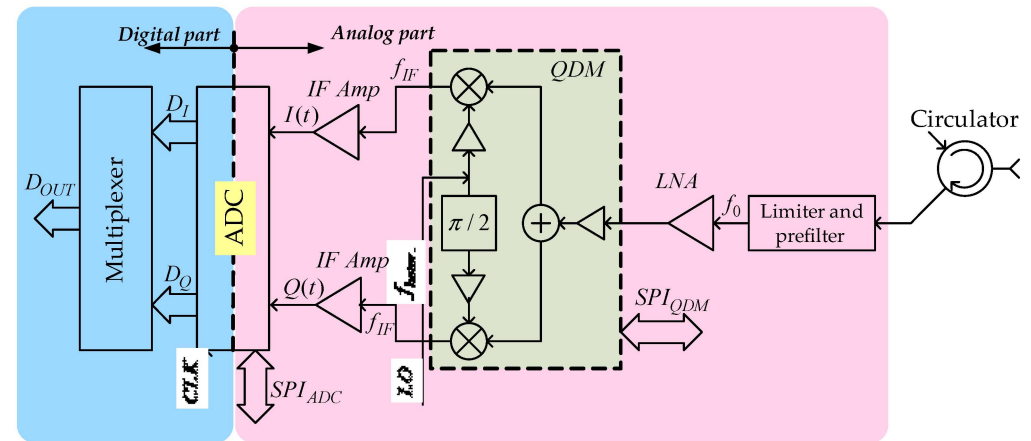


Figure 2. The fundamental structure of the receiving path in the DTM. QDM—quadrature demodulation; LNA—low-noise amplifier; IF Amp—intermediate-frequency (IF) amplifier.

The subsequent characteristics of the receiving path in the DTMs are elucidated through a comparative analysis with the digital receivers employed in the traditional radar systems. This analysis particularly focuses on scenarios involving the observation and detection of objects with low RCSs.

1. Assume that both the traditional radar system and the modern system, utilizing DPAA models, possess the same antenna aperture area, denoted as S_{ant} . Both systems transmit with a power of P_{trans} and have a signal width of t_{sig} . to observe and detect an object with an RCS of $\bar{\sigma}_{object}$ at a maximum distance of R_{max} . while ensuring resolution at a distance of $\sigma_{r_{min}}$. The power level, $P_{r.}$, of the return signal at the input of the digital receiver in the traditional radar model can be determined by the following expression [4–7]:

$$P_{r.} = \frac{P_{trans} \times G_{ant.} \times \bar{\sigma}_{object} \times S_{eff.}}{(4\pi)^2 \times R_{max}^4} \tag{1}$$

where $G_{ant.} = (4\pi/\lambda^2) \times S_{eff.}$ is the antenna amplification factor; $S_{eff.} = v \times S_{ant}$ is the effective area of the antenna; and $v = 0.55 \div 0.82$ is the coefficient of the antenna open surface area.

The conditions for observation and object detection are as follows:

$$P_{r.} \geq P_{r_{min}} \sim P_{inter.noise} \tag{2}$$

where $P_{r.min}$ and $P_{inter.noise}$ represent the minimum power level of the return signal from the object and the power level of the internal noise of the receiver, respectively.

Meanwhile, the digital receiver and the digital receiving path have the same structure, as depicted in Figure 1. Their internal noise power level can be estimated based on the approach coordinating the bandwidth, $\Delta f_{amp.part}$, of the low-noise amplifier (LNA) and the intermediate-frequency amplifier (IFA) with the amplitude spectrum of the signal. This bandwidth is determined by the distance resolution $\sigma_{r.min}$. It is inferred that the power of the internal noise, $P_{inter.noise}$, estimated in terms of $\Delta f_{amp.part}$, is given by the following expression:

$$P_{inter.noise} = kT_0 \times \Delta f_{amp.part} \tag{3}$$

where $k = 1.38 \times 10^{-23}$ J/K and $T_0 = 300$ K are the Boltzmann constant and the absolute noise temperature, respectively.

From this, it can be inferred that, assuming the characteristic data of $\sigma_{r.min}$ lie within the radar frequency range from 30 to 200 [m], the variable $\Delta f_{amp.part}$ is expected to be between 10^7 Hz and 10^6 Hz. This results in the internal noise power level, $P_{inter.noise}$, falling within the range 10^{-15} W to 10^{-14} W.

Therefore, in traditional radar models, the observation and detection of objects with a small RCS present a challenge that requires the full coordination of technical and technological capabilities. This coordination is necessary to appropriately select the parameters P and S to ensure that Expression (2) is realized.

2. In a radar system employing a DPAA integrated with N DTM modules, the power level of the return signal from the object at the input of the receiving path, $P_{r.DTM}$, can be estimated using two methods.

The first method, $P_{r.DTM}$, is estimated according to Expression (1). In this, G_{ant} and S_{eff} are replaced by $G_{an.el.}$ and $S_{eff.an.el.}$, respectively, which represent the gain coefficient of the antenna element coupled to the input of the receiving path and the effective area of that element. The antenna element coupled to the DTM typically takes the form of a half-wavelength antenna, a loudspeaker antenna, or a microstrip antenna. These elements have an amplification factor of $G_{an.el.} \approx 3$, resulting in $S_{eff.an.el.} \approx (3\lambda^2)/4\pi$.

The second method assumes that the electromagnetic field wave of the signal, reflected from the object, behaves like a plane wave. Consequently, the power level $P_{r.DTM}$ is calculated by distributing the power P_r evenly across the modules. The number of modules N_{mod} can be estimated by dividing the open surface area of the antenna S_{ant} by the area of the antenna element $N_{ant.element}$, which is determined by the distance $d \approx 0.6 \times \lambda$ between adjacent DTM modules in both the horizontal and vertical orientations of S_{ant} . For instance, at the L band (approximately 1GHz), given an antenna with an open surface area of $G_{ant.} = 4 \times 6$ m², the number of transceiver modules N_{mod} will be approximately 741 elements.

Table 1 presents the results of the qualitative estimation of parameters $P_{inter.noise}$, and P_r of the traditional models, as well as $P_{r.DTM}$ at the input of the receiving path of DTMs in the DPAA at the typical radar frequency bands, provided that $\bar{\sigma}_{object}$ lies in the range from 0.01 m² to 0.05 m².

Table 1. The results of qualitative estimation of $P_{inter.noise}$, P_r , and $P_{r.DTM}$.

Parameter	VHF-Band	L-Band	X-Band
$P_{inter.noise}$, W	$\sim(6..9) \times 10^{-15}$	$\sim 10^{-15}$	$\sim(1..4) \times 10^{-14}$
P_r , W	$\sim 10^{-15}$	$\sim(8..9) \times 10^{-16}$	$\sim(1..3) \times 10^{-15}$
$P_{r.DTM}$ W	$\sim 10^{-19}$	$\sim 10^{-20}$	$\sim 10^{-21}$

The estimates for $P_{r.DTM}$ in Table 1 show that they are not only small, but also much smaller than the internal noise level.

That is, the signal-to-internal-noise ratio at the input of the DTM is much less than one and is in the range $SNR_{In\ of\ analog.\ part}|_p \sim (10^{-8} \div 10^{-4})$.

$$SNR_{In\ of\ rec.\ path}|_p = SNR_{In\ of\ analog.\ part}|_p = P_{r.DTM}/P_{Inter.noise} \ll 1 \quad (4)$$

Given that the input impedance of the LNA element in the receiving path is Z_{in} , Ohm , the mean square values of the internal noise voltage and the voltage amplitude of the return signal are, respectively,

$$\sigma_{inter.noise\ DTM} = \sqrt{2P_{Inter.noise} \times Z_{in}}, \sigma_{r.DTM} = \sqrt{2P_{r.DTM} \times Z_{in}} \quad (5)$$

It can also be estimated that the internal signal-to-noise ratio will be in the range $SNR_{In\ of\ analog.\ part}|_U \sim (10^{-4} \div 10^{-3})$. This ratio will be even smaller under practical conditions.

The second characteristic inevitably leads to the need for structural re-perfecting (improvement) of the DTM receiving path when modern radar models using DPAAAs perform observations and detect objects with small RCSs.

There are two primary reasons that underscore the necessity for improving the structure of the receiving path.

Firstly, in comparison to the traditional model, each DTM module is paired with an antenna element with a gain of only three, which is significantly lower than that of a large antenna system. For instance, in the L band, with $S_{ant} = 4 \times 6\ m^2$, the antenna gain $G_{ant.} \approx 2.476 \gg G_{an.el.} \approx 3$.

Secondly, because the signal-to-internal-noise ratio at the input of the receiving path is much less than one, the receiving path synthesized by the optimal filtering model is not truly suitable. It is only appropriate when $P_{r.DTM}$ is greater than or equal to $P_{inter.noise}$. In other words, the classical definition of the receiver dynamic range cannot be applied to the receiving path when the modern radar performs observations and detects objects with low RCSs.

It should be noted that the data that are qualitatively estimated above are only for RCSs in the $[dm^2]$ range. Today, radar technology and techniques ensure that objects have RCSs of only a few $[cm^2]$. In this case, the signal-to-internal-noise ratio will be even smaller.

3. Results and Discussion

Based on the contents presented in the second section, the refinement of the receiving path structure commences with an adjustment of its dynamic range concept. This new concept forms the foundation for selecting and adjusting the structure of the receiving path in accordance with the filtering model to satisfy signal processing requirements. The final step involves completing the structure to ensure the capability to observe and detect objects with a low RCS.

3.1. Adjusting the Dynamic Range Concept for the Receiving Path of DTMs

According to radar theory, the traditional definition of the dynamic range of the receiver is the ratio of the maximum to the minimum input signal levels, $U_{up.thres}$ or $U_{r.max}/U_{r.min}$. Within this range, the receiver maintains its operating characteristics, with the characteristic of the linear gain being particularly significant. Here, $P_{r.max}$ and $U_{r.max}$ represent the maximum power and voltage level of the input signal that the receiver can handle without saturation, respectively. Conversely, $P_{r.min}$ and $U_{r.min}$ denote the minimum power and voltage level of the input signal at which the signal-to-noise ratio, $SNR_{In\ of\ rec.}|_p$, $SNR_{In\ of\ rec.}|_U$, equals one. The level of $P_{r.max}$ is limited by the allowable deviation in the amplitude characteristic from linearity and is only respectable in cases where the signal-to-internal-noise ratio at the receiver input exceeds one. However, when

the system performs the observation and detection of objects with a low RCS, such a definition of dynamic range is not entirely suitable for the receiving path.

1. A deep analysis of the structure of the receiving path shows that, in the analog part of the receiving path, when dealing with objects that have low RCSs, the signal-to-noise ratio is significantly less than one. That means that the return signal level is substantially lower than the internal noise level. Therefore, the dynamic range of the analog part of the receiving path must be defined as the range of internal noise voltage values converted to the input.

Due to the symmetry of the return signals and of internal noise relative to the operating point on the amplitude characteristic of the amplifier, the upper and lower threshold voltages, $U_{low.thres}$ and $U_{up.thres}$, respectively, must be selected such that the probability of noise peaks, $P(U_{out\ of\ ana.\ part} | \sigma_{out\ of\ ana.\ part} > U_{up.thres})$, is the probability of a noise peak at the output of the analog part, given that the noise peak exceeds U_{noise} , and $P(U_{out\ of\ ana.\ part} | \sigma_{out\ of\ ana.\ part} < U_{low.thres})$ is the probability of a noise peak at the output of the analog part, given that the noise peak is less than U_{noise} , approaching zero.

Specifically, during the synthesis of the structure for the analog part at receiving path, the selected design is based on the abovementioned treatment. That is, $U_{up.thres} - U_{Op.point} = k \times \sigma_{inter.noise\ DTM}$ and $U_{low.thres} - U_{Op.point} = -k \times \sigma_{inter.noise\ DTM}$. Once the magnitude of $\sigma_{inter.noise\ DTM}$ is estimated, we can easily determine k so that the two probabilities have very small values. For example, at the L band, with $k = 5 \div 6$, $P(U_{out\ of\ ana.\ part} | \sigma_{out\ of\ ana.\ part} > U_{up.thres}) \sim P(U_{out\ of\ ana.\ part} | \sigma_{out\ of\ ana.\ part} < U_{low.thres}) \approx 10^{-7}$, and can be ignored.

Then, $U_{up.thres} = U_{Op.point} + (5 \div 6) \times \sigma_{inter.noise\ DTM}$, $U_{low.thres} = U_{Op.point} - (5 \div 6) \times \sigma_{inter.noise\ DTM}$, and $U_{Op.point}$ are the positions of the operating point (Figure 3a). In addition, the dynamic range of the analog part, quantitatively, can be estimated by the following expression:

$$D = 20 \times \log(U_{up.thres} / U_{low.thres}) \tag{6}$$

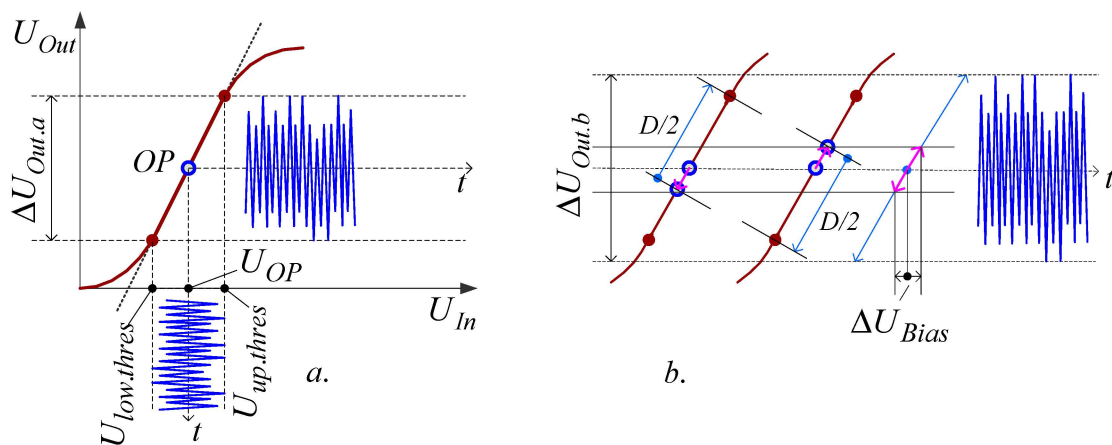


Figure 3. Determining the dynamic range for the analog part of the receiving path (a), and the adaptive adjustment of the operating point position (b).

That is, the dynamic range of the analog part of the receiving path is dictated by the complete spectrum of noise peak variations. The design of the analog part must ensure that its dynamic range matches the range of internal noise fluctuations. This requirement ensures that even when the return signals are minimal, their characteristic parameters (as phase and amplitude) are inherently maintained as they traverse this part.

Consequently, as the signal progresses through the analog part, potential errors in the phase and amplitude parameters must be minimized to a specified level to guarantee the effectiveness of subsequent processing. Adjusting the concept of the dynamic range of

the analog part as stated above allows its structure to be re-perfected from an optimal to a matched filter model [20].

2. This is the digital part in the receiving path, with the input element being the ADCs. Consequently, analogous to conventional digital receivers, the input signal range of the ADC must align with the voltage variation range at the output of the analog part. This necessitates that the voltage variation range at the output of the analog part be less than the nominal input range of the ADC, as stipulated in its datasheet.

The primary parameters of the ADC that must be considered when matching the output of the analog part include the nominal full-scale voltage range of the ADC, denoted as ΔU_{ADC} , and the quantization step h_{ADC} , also referred to as the value of the least significant bit.

$$\Delta U_{ADC} > \Delta U_{Out.analog.part}; h_{ADC} = (\Delta U_{ADC})/2^p \quad (7)$$

where p is the number of bits of the ADC.

Thus, the dynamic range of the digital part is the dynamic range of the ADC:

$$D_{Dig.part} = D_{ADC} = \Delta U_{ADC}/h = 2^p \quad (8)$$

In principle, the quantization step h serves as the parameter that assesses the sensitivity of the ADC. Consequently, its magnitude must be at least an order of magnitude smaller than the amplitude of the input signal.

Specifically, the L band, as indicated by Table 1 and Equation (5), can be estimated as $U_{r.DTM} \sim 10^{-9}$ V. If an analog gain of approximately $K_U \sim 10^3$ occurs, then the value of h_{ADC} will be

$$h_{ADC} = (K_U \times U_{r.DTM})/10 \approx 10^{-7} \text{ V}$$

Additionally, the total noise voltage fluctuation at the output of the analog part can also be estimated using the data from Table 1 and Equation (5):

$$U_{noise \text{ at Out of amp.part}} = 10 \times K_U \times \sigma_{int.noise.DTM} \approx 3.16 \times 10^{-3} \text{ V}$$

The full-scale voltage range of the ADC, ΔU_{ADC} , must be taken to be greater than the $U_{noise \text{ at Out of amp.part}}$ value. For example, if we assign $\Delta U_{ADC} = 3.3 \times 10^{-3}$ V, then the number of bits of the ADC is determined from the following equation:

$$\Delta U_{ADC} = h_{ADC} \times 2^p = 10^{-7} \times 2^p = 3.3 \times 10^{-3} \text{ V}$$

If $p = 15$ is chosen, ΔU_{ADC} will be slightly below the required threshold. In addition, if $p = 16$ is selected, the estimated $dU(ADC)$ will exceed the requirement by a significant margin. However, to ensure a certain match between the digital and analog parts, a value of $p = 16$ is adopted.

Re-evaluation gives the following:

$$\Delta U_{ADC} = 10^{-7} \times 2^{16} = 6.55 \times 10^{-3} > 3.3 \times 10^{-3} \text{ V}$$

For contemporary ADCs, the size of the achievable minimum quantization step is contingent upon the signal magnitude that the amplifier in the analog part must deliver. Consequently, it is advisable to synthesize the analog part with multiple low-noise, matched amplifier stages. Nevertheless, excessively broadening the dynamic range of the ADC can introduce several limitations, including signal distortion caused by the amplifier elements and an increased nonlinearity in the transfer function during the encoding process of the ADC.

In summary, the two subsections above detail the research results in improving the structure of the receiving path by transitioning from an optimal filter model to a fully matched filter model. This is to enable the detection of objects with a small RCS. The core issue of "matching" addressed here involves redefining the concept of dynamic range to optimize the structure, ensuring that the return signals are not distorted and that potential

parameter errors of the amplitude and phase are maintained within acceptable limits. This approach enhances the efficiency of filtering and the subsequent accumulation of weak signals.

Nevertheless, the challenge of dynamic range requires careful consideration in radar systems, which must detect objects with the common RCS while also accounting for the impact of external noise. Consequently, the structural improvement in the receiving path should be performed using an adaptively controlled dynamic range approach.

3.2. Improvement in the Structure of the Receiving Path Using Adaptively Controlled Dynamic Range

Upon analyzing the functions of each component within the receiving path, it becomes evident that the analog parts, particularly the intermediate-frequency (IF) amplifiers, are crucial in maintaining the amplification factor throughout the system. Specifically, it ensures the linearity of the entire receiving path. Consequently, the primary focus of perfecting should be the analog part. Furthermore, the receiving path in the DTM must also guarantee performance for objects with common RCS values. This necessitates the detection of objects with the covering of an RCS range from $\bar{\sigma}_{object.small} \sim (0.01 \div 0.05) \text{ m}^2$ to $\bar{\sigma}_{object.com} \geq 1.5 \text{ m}^2$. That is, the receiving path must be adaptable to account for those variations. Furthermore, the correspondence between the analog and digital parts can be characterized as a “rigid matching” model. Therefore, the solution involving an adaptive controlled dynamic range should be applied to the analog part.

Accordingly, to ensure adaptive control, we propose utilizing a feedback mechanism in which input information is derived from the output data of the digital part. They are processed according to the proposed function to become control signals for the operation of the analog part.

The proposed model is presented in Figure 4 and is explained as follows: Following its passage through the down-mixer, the return signal is directed to the adder at the intermediate frequency (IF) to supplement the voltage from the output of the DAC, initially set to zero. This DAC element is located in the compensation (offset) voltage generation unit (OVGU). Subsequently, the signal is amplified and digitized by the amplifier element and the ADC. The digitized data (in code format) are then transmitted to the microprocessor and control unit (M&CU), which estimates the data sample of the signal at the amplifier’s output. When these data remain within the limits corresponding to the amplifier’s operational range in the unsaturated mode (i.e., within the linear range), the M&CU generates an appropriate code. This code is subsequently fed to the DAC (in the OVGU) to generate a compensation voltage. This voltage is formed so that, when added to the return signal, the IF signal at the output of the adder is linearly amplified by the IF preamplifier in the analog part, and synthesized according to the model of an amplifier with an adaptively controlled bias voltage. The ADC’s estimation of the subsequent data sample follows the same procedure.

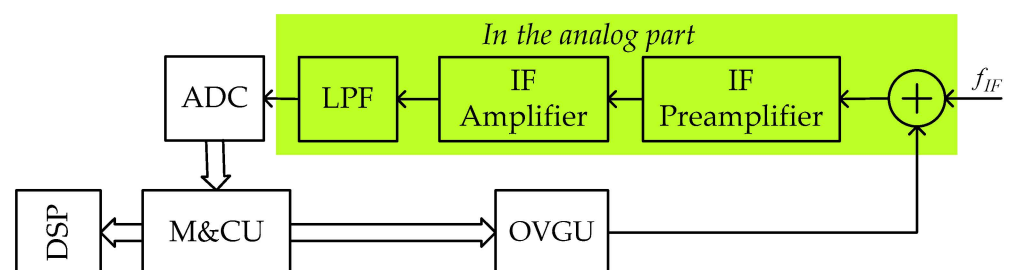


Figure 4. The model proposed for improving the structure of the analog part in the DTM. M&CU—microprocessor and control unit; OVGU—offset voltage generation unit; LPF—low-pass filter.

The output code from the ADC and the input code of the DAC are transmitted from the M&CU to the digital signal processing unit (DSP) to perform the addition and to recover

the data of the return signal. In the model, the adder is synthesized using an operational amplifier (*Opamp*) ADL5331, which is fabricated on an Analog Devices in United States, with its slew rate (SR) being a crucial characteristic parameter, estimated by the following expression:

$$SR = \max \left[\frac{\partial U_{out.Opam.(t)}}{\partial t} \right] \tag{9}$$

where $U_{out.Opam.(t)}$ is the output voltage function of the *Opamp* depending on time.

The parameter SR of the *Opamp* must also satisfy the condition $SR \geq 2\pi f \times U_{peak}$, where f, U_{peak} are the frequency and peak value of the signal amplitude at the output, respectively. Thus, the slew rate of the output voltage allows us to estimate the maximum frequency of the input signal at which the output signal remains undistorted.

This implies that the parameters of the *Opamp* functioning as an adder are crucial for ensuring that the preamplifier in the analog part operates in amplifier mode with the adaptive controlled bias voltage.

In the model, on the basis of a comparison between the value of the ADC’s output data, $\Delta U_{Out\ of\ ADC}$, and its nominal maximum value, $\Delta U_{Out\ of\ ADC\ nom.}$, one of three commands is given: the “0” command (meaning no compensation), the offset command “ $+U_{comp.}$ ”, and the offset command “ $-U_{comp.}$ ”. The amount of compensation is estimated by the factor $K_{ADC} = \Delta U_{Out\ of\ ADC} / \Delta U_{Out\ of\ ADC\ nom.}$, and is performed according to the input signal sampling rate. To ensure that the input range of the ADC firmly matches with the output range of the analog part, the value of K_{ADC} is usually set to 0.7. Thus, the adaptive control period corresponds to the duration of an input signal sample. The addition of the compensation voltage is performed in the negative input value region of the signal and vice versa. Thus, the adaptive control of the compensation voltage applied to the input of the adder element results in a corresponding adaptive modification of the bias voltage (Figure 3b) (i.e., adaptive adjustment of the operating point on the linear part of the amplitude characteristic) of the IF preamplifier. Correspondingly, the dynamic range of the analog part is adaptively controlled. Thus, it can be stated that the dynamic range of the receiving path is adaptively “pseudo-expanded”. Figure 5 presents the general structure of a DTM system employing quadrature modulation, highlighting the implemented enhancements aimed at minimizing amplitude and phase errors in the return signals as they traverse the reception path.

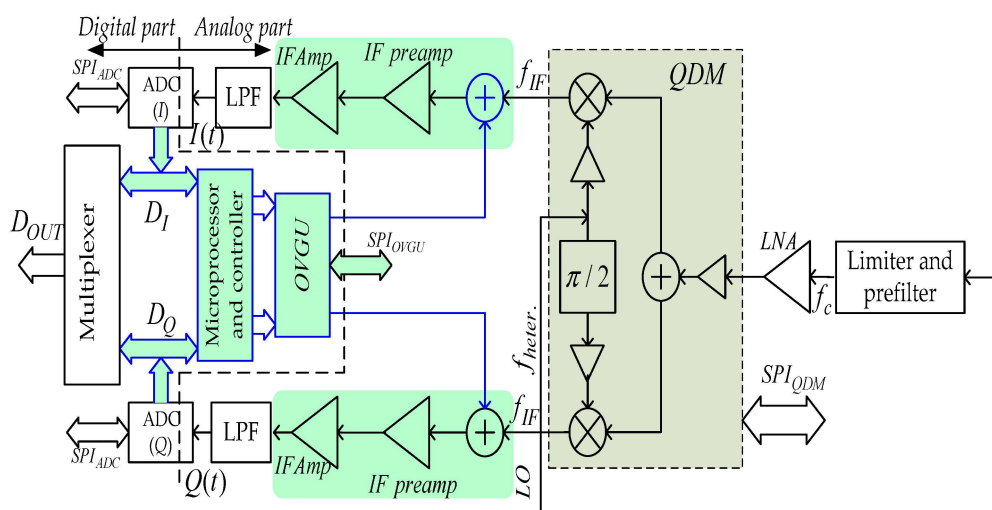


Figure 5. The general structure of a DTM system using quadrature modulation after the improvement in the receiving path. QDM—quadrature demodulation; LNA—low-noise amplifier; IF preamp—IF preamplifier.

3.3. Simulation Procedure and Interpretation of Expressions for Estimating Amplitude and Phase Errors

Minimizing the phase and amplitude errors in the return signals from objects with small RCSs enhances the efficiency of signal accumulation both spatially and temporally. Consequently, the primary objective of the simulations presented in this study is to qualitatively demonstrate the effectiveness of the proposed improvements to the receiver path structure in reducing these phase and amplitude errors, as theoretically outlined in earlier sections. A secondary objective is to qualitatively assess the impact of these improvements on the accumulation of signals and their subsequent contribution to the detection of objects with small RCSs. Moreover, because the receiving path structure model employs quadrature demodulation, with its two I and Q channels being functionally identical, it is sufficient to conduct simulations for the analog path on one channel to demonstrate the theoretical results. Consequently, considering these recommendations and the research findings presented in [21,22], a simulation procedure can be developed, as depicted in Figure 6.

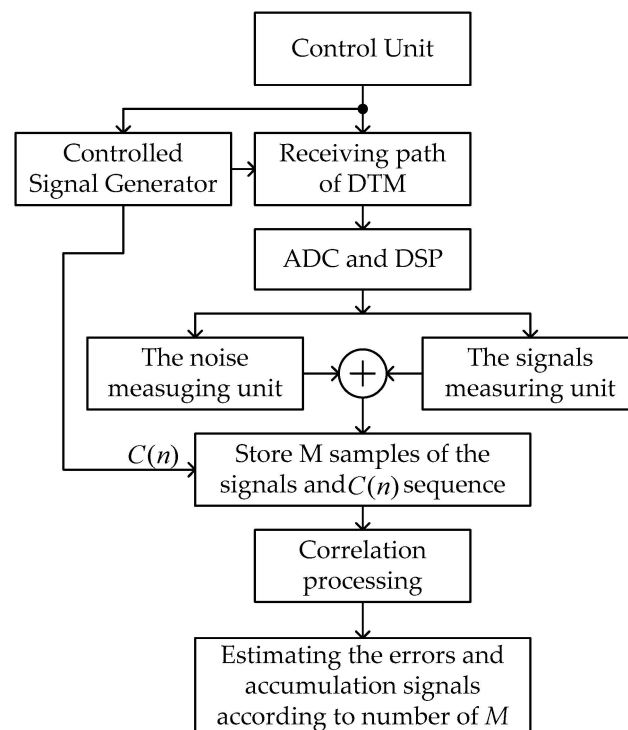


Figure 6. The simulation procedure.

Under the supervision of the control unit, the controlled signal generator (CSG) produces a signal that is subsequently directed to the input of the receiving path. The IF signal is digitized and split into two branches, which are utilized to measure the magnitude of the internal noise and the signal, which is employed to adjust the signal level relative to the noise during the simulation. The resulting signal data, along with the corresponding data representing the mirror image of the transfer function, are simultaneously recorded in the buffer register designated for correlation processing. When the buffer accumulates a sufficient number of samples M , correlation processing is conducted to estimate the phase and amplitude errors. This process also facilitates a qualitative evaluation of the effectiveness of data accumulation for both the “non-expanded” and the adaptively “pseudo-expanded” scenarios of the linear gain range in the analog part of the receiving path.

For simplicity, let us assume that the radar model uses a signal modulated by a phase-shift keying (PSK) code with N positions. Consequently, in the absence of external interference, the signal in the receiving path can be expressed as follows:

$$S_{rec.path}(n) = S_{CSG}(n) + N(n) \tag{10}$$

where $S_{CSG}(n), N(n) = N_I(n) + jN_Q(n)$ are the CSG-generated signal and the internal noise, respectively.

$$S_{CSG} = [U \times \exp(j\varphi)] \times C(n) \tag{11}$$

where $U, \varphi, C(n) = \pm 1$ are the amplitude, phase of the signal in the receiving path, and the binary modulation code sequence of the phase, respectively.

To achieve signal separation in the receiving path, the received signal $S_{rec.path}(n)$ in (10) is multiplied by $C(n)$, resulting in the following expressions:

$$\tilde{S}_{rec.path}(n) = S_{rec.path}(n) \times C(n) = U \times \exp(j\varphi) + [S_{I.noise}(n) + jS_{Q.noise}(n)] \times C(n) \tag{12}$$

$$\tilde{S}_{rec.path}(n) = U \times \exp(j\varphi) + \tilde{S}_{I.(noise+logr)}(n) + j\tilde{S}_{Q.(noise+logr)}(n) \tag{13}$$

Therefore, assuming that other effects are negligible, it can be inferred from Expression (12b) that $\tilde{S}_{rec.path}(n)$ encapsulates information regarding the amplitude and phase of the signal as it traverses the receiving path. Additionally, the components $\tilde{S}_{I.(noise+logr)}(n)$ and $\tilde{S}_{Q.(noise+logr)}(n)$ contain errors arising from internal noise and the limitations of the linear gain range. Let $\sigma_{I.(noise+logr)}^2$ and $\sigma_{Q.(noise+logr)}^2$ represent the variances of the sample sequences $\tilde{S}_{I.(noise+logr)}(n)$ and $\tilde{S}_{Q.(noise+logr)}(n)$, respectively. Thus, the errors are defined as three times the standard deviation. Therefore, we obtain

$$\tilde{S}_{rec.path}(n) = U \times \exp(j\varphi) \pm [3\sigma_{I.(noise+logr)} + j3\sigma_{Q.(noise+logr)}] \tag{14}$$

According to [23], the random error decreases after many accumulations. Specifically, with M accumulations, the errors and the standard deviation decrease by \sqrt{M} .

This means that

$$\overline{\tilde{S}_{rec.path}} = U \times \exp(j\varphi) \pm \frac{[3\sigma_{I.(noise+logr)} + j3\sigma_{Q.(noise+logr)}]}{\sqrt{M}} = [U \times \cos(\varphi) \pm \frac{3\sigma_{I.(noise+logr)}}{\sqrt{M}}] + j[U \times \sin(\varphi) \pm \frac{3\sigma_{Q.(noise+logr)}}{\sqrt{M}}] \tag{15}$$

It is appropriate and sufficiently general to assume that $\sigma_{I.(noise+logr)} = \sigma_{Q.(noise+logr)} = \sigma_{(noise+logr)}$ and Expression (13) can be abbreviated as

$$\overline{\tilde{S}_{rec.path}} = U \times \exp(j\varphi) \pm \frac{3\sigma_{(noise+logr)}(1 + j)}{\sqrt{M}} \tag{16}$$

By normalizing the power level of the signal from the CSG with respect to the internal noise ($U^2 \rightarrow \sigma_{noise}^2$), and subsequently, transforming Expression (14), we obtain

$$\overline{\tilde{S}_{rec.path.norm}} = \exp(j\varphi) \pm \frac{3\sigma_{(noise+logr)}(1 + j)}{\sqrt{M}} = \exp(j\varphi) \pm \frac{3\sigma_{(noise+logr)}}{\sqrt{M}} \exp(j\frac{\pi}{4}) \tag{17}$$

Hence, Expression (16) below is the basis for estimating the error of the amplitude and phase of the signal when passing through the analog part of the receiving path (according to two variables M and $\sigma_{(noise+logr)}$) corresponding to before and after the improvement:

$$F = \frac{\tilde{S}_{rec.path.normal}}{\exp(j\varphi)} = 1 \pm \frac{3\sqrt{2}\sigma_{(noise+logr)}(1+j)}{\sqrt{M}} \cos\left(\frac{\pi}{4} - \varphi\right) \pm j \frac{3\sqrt{2}\sigma_{(noise+logr)}(1+j)}{\sqrt{M}} \sin\left(\frac{\pi}{4} - \varphi\right) \quad (18)$$

Considering the scenario with the largest error (i.e., $\pm \cos(\frac{\pi}{4} - \varphi) = 1$), the amplitude error can be determined from Equation (16) and expressed by the following equation:

$$\delta_U [dB] = |F|^2 [dB] = 10 \log \left[1 + \frac{18\sigma_{noise+logr}^2}{M} + \frac{6\sqrt{2}\sigma_{noise+logr}}{\sqrt{M}} \right], [dB] \quad (19)$$

Similarly, considering the scenario with the largest error (i.e., $\pm \sin(\pi/4 - \varphi) = 1$), the phase error is

$$\delta_U = |Arg(F)| = \left| Arg \left[1 + j \frac{3\sqrt{2}\sigma_{(noise+logr)}}{\sqrt{M}} \right] \right|, \quad (20)$$

Equations (18) and (19) present the results for estimating the amplitude and phase errors of the signal within the receiving path, before and after the implementation of our proposed structural improvements.

3.4. Simulation Results and Comments

Figure 7a,b present examples of simulation results of the additive mixture of a signal modulated by an $N = 1024$ -position phase-shift keying (PSK) code and internal noise with varying $U_{signal}/\sigma_{noise}$ values. When $U_{signal}/\sigma_{noise}$ is 0.1, as shown in Figure 7a, the signal-to-noise ratio at the input of the receiving path, $SNR_{In\ of\ rec.\ path}|_p$, according to Expression (4), is approximately equal to 0.01. Assuming that the objects have a common RCS with $\bar{\sigma}_{object} \sim 1.0\ m^2$ and that the power level of the return signal equals the internal noise level, $SNR_{In\ of\ rec.\ path}|_p \sim 1$, we can consider the simulation to have been conducted for an object with an RCS corresponding to $\bar{\sigma}_{object} \sim 0.01\ m^2 = 1\ dm^2$. Analogous to Figure 7b, when the ratio $U_{signal}/\sigma_{noise}$ is 0.05, it can be inferred that the radar is detecting objects with a small RCS of $\bar{\sigma}_{object} \sim 2.5\ cm^2$.

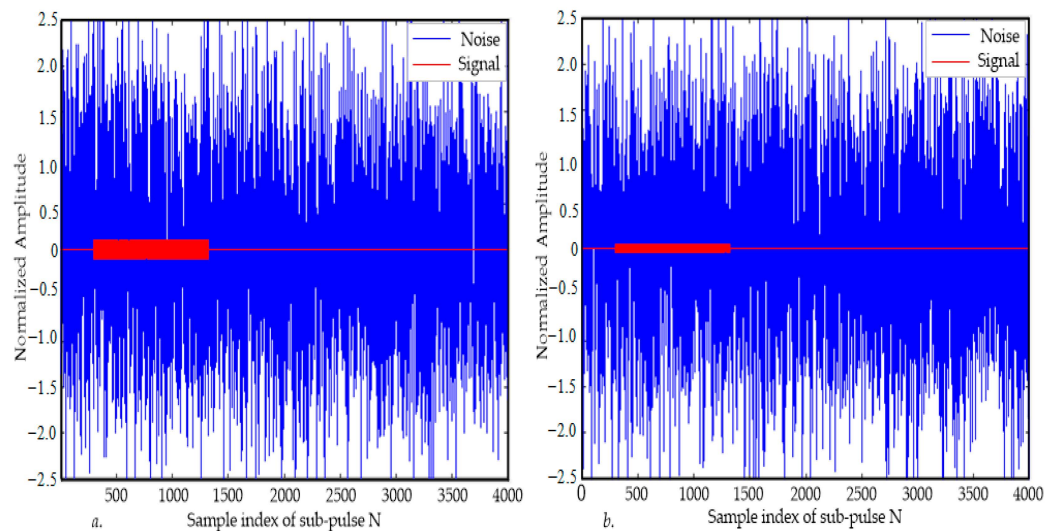


Figure 7. The additive mixture simulation results of signals modulated by phase-shift keying code with 1024 positions and internal noise: (a) $\tau_{signal}/\tau_{sub-pul} = 1024$, $U_{signal}/\sigma_{noise} \sim 0.1$; (b) $\tau_{signal}/\tau_{sub-pul} = 1024$, $U_{signal}/\sigma_{noise} \sim 0.05$.

Tables 2 and 3 provide detailed simulation results of amplitude and phase error data across two scenarios, both before and after the enhancement in the receiving path. The

results are presented for two distinct cases, corresponding to the ratios $U_{signal}/\sigma_{noise} \sim 0.1$ and $U_{signal}/\sigma_{noise} \sim 0.05$.

Table 2. These data show the results of estimating the amplitude error of the signal before (*) and after (**) the improvement in the receiving path.

		Amplitude Error [dB]								
$M = (x) \times 10^3$		3.5	4.0	4.5	5.0	5.5	6.0	6.5	7.0	7.5
$U_{signal}/\sigma_{noise} \sim 0.1$	(*)	0.91	0.88	0.86	0.85	0.83	0.78	0.79	0.78	0.77
	(**)	0.72	0.69	0.68	0.64	0.64	0.63	0.62	0.61	0.61
$U_{signal}/\sigma_{noise} \sim 0.05$	(*)	0.61	0.57	0.52	0.50	0.45	0.43	0.41	0.40	0.38
	(**)	0.44	0.42	0.41	0.38	0.38	0.36	0.35	0.34	0.35

Table 3. These data show the results of estimating the phase errors of the signal before (*) and after (**) the improvement in the receiving path.

		Phase Error [Degree]								
$M = (x) \times 10^3$		3.5	4.0	4.5	5.0	5.5	6.0	6.5	7.0	7.5
$U_{signal}/\sigma_{noise} \sim 0.1$	(*)	7.67	6.85	6.77	6.66	6.52	6.31	6.46	6.26	6.27
	(**)	6.51	6.25	6.13	5.88	5.86	5.62	5.55	5.61	5.63
$U_{signal}/\sigma_{noise} \sim 0.05$	(*)	6.15	5.84	5.63	5.33	4.77	4.52	4.26	3.89	3.81
	(**)	5.16	4.88	4.72	4.33	4.21	3.93	3.56	3.33	3.24

Figure 8 illustrates the graphs of amplitude error (Figure 8a) and phase error (Figure 8b) estimates, evaluated over M accumulations ranging from 3.5×10^3 to 7.5×10^3 , before (dashed lines) and after (solid lines) the improvement in the receiving path. These graphs are presented for two distinct cases, corresponding to the ratios of $U_{signal}/\sigma_{noise} \sim 0.1$ (green) and $U_{signal}/\sigma_{noise} \sim 0.05$ (pink).

To qualitatively assess the effectiveness of the receiving path improvement, Figure 9 presents the simulation results of signal accumulation for the case where $M \sim 6 \times 10^3$ before and after the improvement in the receiving path, corresponding to accumulation ratios of $U_{signal}/\sigma_{noise} \sim 0.1$ and $U_{signal}/\sigma_{noise} \sim 0.05$, respectively.

The simulation software was developed using the MATLAB 2024a/Simulink tool of MathWorks in United States [21–26].

Based on the simulation results, the following comments and notes can be made.

First, the correctness of the structure improvement in the receiving path within the DTM has been demonstrated. The reduction in amplitude and phase errors of the return signals after the improvement and completion of the receiving path has allowed the accumulation efficiency to be increased, leading to an increase in the ability to observe and detect objects with small RCSs (Figure 9a compared to Figures 9b and 9c compared to Figure 9d).

Second, for two objects with small RCSs, the object with the larger ratio $U_{signal}/\sigma_{noise}$ will have smaller cumulative errors (green vs. pink in the graph of Figure 8a,b). In addition, compared to reducing amplitude errors, it seems that improving the structure of the receiving path is more effective in reducing phase errors.

Third, a low return signal level relative to the internal noise of the received path has been observed not only for objects with small RCSs, but also for those with typical RCSs at medium and long observation distances. Consequently, the enhancement in the receiving path structure also contributes to the further improvement in the ability to observe and detect common objects.

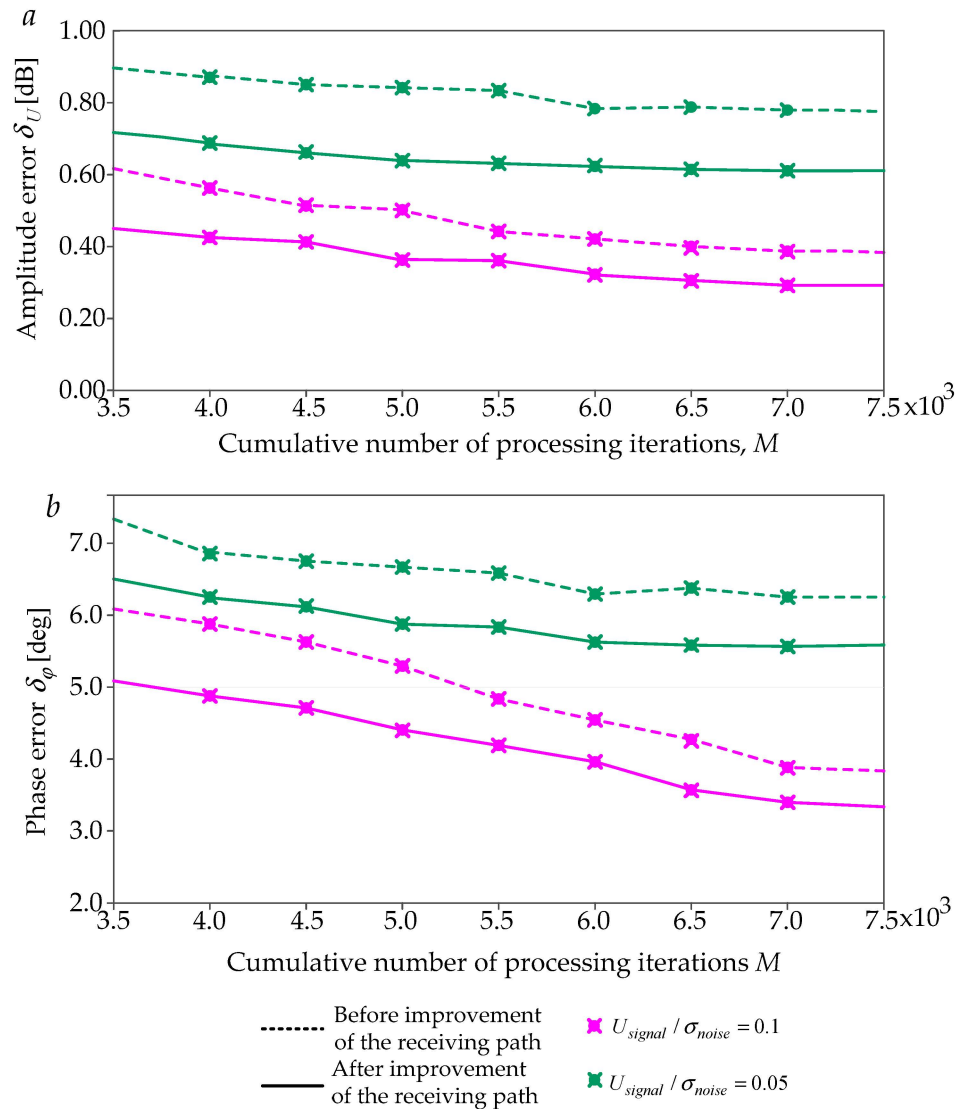


Figure 8. The amplitude (a) and phase errors (b) of the return signals before and after the improvement in the receiving path in the DTM.

Third, a low return signal level relative to the internal noise of the received path has been observed not only for objects with small RCSs, but also for those with typical RCSs at medium and long observation distances. Consequently, the enhancement in the receiving path structure also contributes to the further improvement in the ability to observe and detect common objects.

Fourth, in principle, employing a receiving path structure where the analog section is based on the superheterodyne receiver model does not compromise the generality of the approach in the improvement process. The detailed realization of the structural enhancements depends entirely on the technical and technological capabilities, the expertise of the designer and manufacturer, and the availability of materials and components. It is important to emphasize that the proposed improvements to the receiving path structure do not necessitate the addition of components or an increase in the size and mass of the DTM.

Fifth, a key feature of the receiving paths in modern DTMs within DPAA systems is their synthesis based on quadrature demodulation. Consequently, their performance and quality are highly dependent on the balance between the I and Q channels, which is maintained by the calibration subsystem integrated within the DTM. This subsystem is relevant to varying extents in relation to the previously discussed improvements, particularly in the generation of the offset voltages serving different functions.

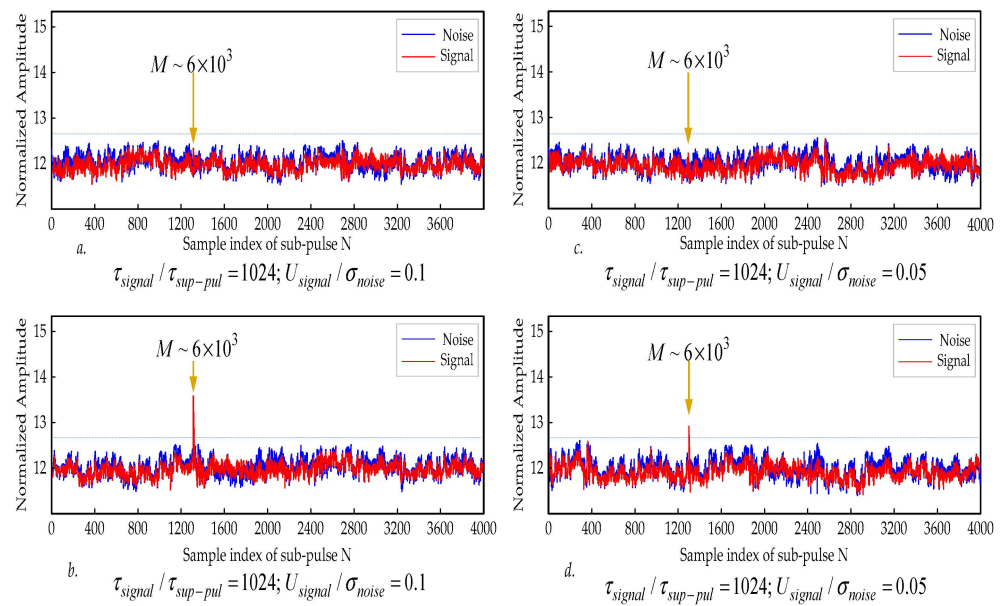


Figure 9. The simulation results of signal accumulation when $M \sim 6 \times 10^3$ before and after the improvement in the receiving path in the DTM: (a,b) $U_{\text{signal}} / \sigma_{\text{noise}} \sim 0.1$; (c,d) $U_{\text{signal}} / \sigma_{\text{noise}} \sim 0.05$.

4. Conclusions

This study addresses the challenge of improving the structure of the receiving path in the DTMs of modern DPAA systems to improve the detection of objects with low RCSs, which are inherently difficult to detect. Through a comparative analysis supported by qualitative calculations, we propose a novel approach to modify the receiving path structure, transitioning from an optimal filtering model to a fully matched filtering model. To achieve this, the concept of dynamic range in the receiving path is adapted to scenarios where the signal levels from such objects are significantly lower than the internal noise levels.

The results have created the premise for the proposal of “pseudo-expansion” of the linear gain range of the analog part of the receiving path. The improvement has allowed for a reduction in the amplitude errors and phase errors of the low signals reflected from objects with low RCSs, as demonstrated by the simulation results. This enhancement leads to improved signal accumulation, thereby increasing the signal-to-noise ratio (SNR_{Σ}) at the input of the digital detector of the radar system. Under optimal conditions, where intermodulation distortion noise between DTMs is minimized, the SNR_{Σ} value has the potential to approach the value of $10 \log_{10}(N)_{mod}$.

It is important to note that the detection of low-RCS objects remains a significant challenge, necessitating the integration of various approaches for an effective solution. Among these, the improvement of the receiving path structure, as proposed in this paper, offers a promising approach that should be considered and applied in the research and design of modern multi-functional radar systems to ensure the capability to detect a wide range of object types.

Author Contributions: Conceptualization, X.L.N. and P.B.N.; methodology, X.L.N. and P.B.N.; software, V.H.T.; validation, X.L.N., P.B.N. and T.T.D.T.; formal analysis, T.T.D.T.; investigation, X.L.N.; resources, X.L.N.; data curation, X.L.N.; writing—original draft preparation, X.L.N.; writing—review and editing, P.B.N. and V.H.T.; visualization, X.L.N.; supervision, T.T.D.T.; project administration, T.T.D.T.; funding acquisition, X.L.N. All authors have read and agreed to the published version of the manuscript.

Funding: This research received no external funding.

Data Availability Statement: The original contributions presented in the study are included in the article.

Acknowledgments: The authors would like to thank the anonymous reviewers and editors for providing valuable suggestions and comments.

Conflicts of Interest: The authors declare no conflicts of interest.

References

1. Shestakow, N.V. A Study of Radar Reflections from Low RCS Unmanned Aerial Vehicles. *J. Izv. Tula State Univ. Tech. Sci.* **2022**, *2*, 402–407.
2. Zikidis, K.; Skondras, A.; Tokas, C. Low Observable Principles, Stealth Aircraft and Anti-Stealth Technologies. *J. Comput. Model.* **2014**, *4*, 129–165.
3. Chowdhury, M.-U.-S.; Tahmid, A.; Azmain, M.A.; Chowdhury, M.S.; Hossam-E-Haider, M. Evolution of Algorithms Proposed for Airborne Low RCS Target Detection. In Proceedings of the 2022 IEEE 7th International Conference for Convergence in Technology (I2CT), Mumbai, India, 7–9 April 2022; pp. 1–8. [CrossRef]
4. Barton, D.K. *Radar Equations for Modern Radar*; Artech House: Boston, MA, USA; London, UK, 2013; ISBN 13 978-1-60807-521-8.
5. Richards, M.A.; Scheer, J.A.; Holm, W.A. (Eds.) *Principles of Modern Radar*; Vol. I: Basic Principles; SciTech Publishing: New York, NY, USA, 2010; ISBN 978-1-891121-52-4.
6. Herd, J.; Carlson, D.; Duffy, S.; Weber, M.; Brigham, G.; Rachlin, M.; Cursio, D.; Liss, C.; Weigand, C. Multifunction Phased Array Radar (MPAR) for aircraft and weather surveillance. In Proceedings of the 2010 IEEE Radar Conference, Arlington, VA, USA, 10–14 May 2010; pp. 945–948. [CrossRef]
7. Boric-Lubecke, O.; Lubecke, V.M.; Droitcour, A.D.; Park, B.-K.; Singh, A. Radar Principles. In *Doppler Radar Physiological Sensing*; Wiley: Hoboken, NJ, USA, 2016; pp. 21–38. [CrossRef]
8. Abidi, A.A. The Path to the Software-Defined Radio Receiver. *IEEE J. Solid-State Circuits* **2007**, *42*, 954–966. [CrossRef]
9. Cordeiro, R.F.; Prata, A.; Oliveira, A.S.R.; Vieira, J.M.N.; De Carvalho, N.B. Agile All-Digital RF Transceiver Implemented in FPGA. *IEEE Trans. Microw. Theory Tech.* **2017**, *65*, 4229–4240. [CrossRef]
10. Li, G.; Cai, D. Design of digital transceiver unit based on multi-channel signal synthesis and new filter combination. In Proceedings of the 2017 IEEE 3rd Information Technology and Mechatronics Engineering Conference (ITOEC), Chongqing, China, 3–5 October 2017; pp. 485–488. [CrossRef]
11. Fulton, C.; Yearly, M.; Thompson, D.; Lake, J.; Mitchell, A. Digital Phased Arrays: Challenges and Opportunities. *Proc. IEEE* **2016**, *104*, 487–503. [CrossRef]
12. Harker, B.J.; Dobrosavljevic, Z.; Craney, E.P.; Miles, S.; Belcher, R.A.; Chambers, J. Dynamic Range Enhancements in Radar Sensors PAPER A23. In Proceedings of the 4th EMRS DTC Conference, Edinburgh, UK, 20 July 2007.
13. Harker, B.J.; Dobrosavljevic, Z.; Craney, E.P.; Tubb, C.M.; Harris, G.L. Dynamic range improvements and measurements in radar systems. *IET J.* **2007**, *1*, 398–406. [CrossRef]
14. Peccarelli, N.; James, B.; Fulton, C.; Goodman, N. Dynamic Range Considerations for Modern Digital Array Radars. In Proceedings of the 2020 IEEE International Radar Conference (RADAR), Washington, DC, USA, 28–30 April 2020; pp. 578–583. [CrossRef]
15. Denisov, A.; Danilaev, D.P. Dynamic Range of a Digital Radio Receiver with a Photonic Analog-to-Digital Converter. *J. Pap. Kazan Natl. Res. Tech. Univ.* **2023**, *26*, 77–85. [CrossRef]
16. Goodman, J.; Miller, B.; Herman, M.; Vai; Monticciolo, P. Extending the dynamic range of RF receivers using nonlinear equalization. In Proceedings of the 2009 International Waveform Diversity and Design Conference, Kissimmee, FL, USA, 8–13 February 2009; pp. 224–228. [CrossRef]
17. Poberezhskiy, Y.S. On Dynamic Range of Digital Receivers. In Proceedings of the 2007 IEEE Aerospace Conference, Big Sky, MT, USA, 3–10 March 2007; pp. 1–17. [CrossRef]
18. Raja Abdullah, R.S.A.; Alhaji Musa, S.; Abdul Rashid, N.E.; Sali, A.; Salah, A.A.; Ismail, A. Passive Forward-Scattering Radar Using Digital Video Broadcasting Satellite Signal for Drone Detection. *Remote Sens.* **2020**, *12*, 3075. [CrossRef]
19. Cheng, W.; Zhang, Q.; Lu, W.; Wang, H.; Liu, X. An Efficient Digital Channelized Receiver for Low SNR and Wideband Chirp Signals Detection. *Appl. Sci.* **2023**, *13*, 3080. [CrossRef]
20. Meikle, H. *Modern Radar Systems*, 2nd ed.; Artech House: Norwood, MA, USA, 2008; ISBN 13 978-1-59693-242-5.
21. Viet, H.T.; Minh, T.H. A Real-Time Internal Calibration Method for Radar Systems Using Digital Phase Array Antennas. In *Industrial Networks and Intelligent Systems*; Vo, N.S., Hoang, V.P., Vien, Q.T., Eds.; INISCOM; Lecture Notes of the Institute for Computer Sciences, Social Informatics and Telecommunications Engineering; Springer: Cham, Switzerland, 2021; Volume 379. [CrossRef]
22. Hung, T.V.; Thien, H.M.; Van Bac, N.; Nguyen, P.B. Synthesis of Algorithms and Procedures for Real-Time Internal Calibration of Receiving Channels in Digital Phased Antenna Arrays. *J. Russ. Univ. Radioelectron.* **2022**, *25*, 64–73. [CrossRef]
23. MATLAB & Simulink. Available online: <https://www.mathworks.com/help/simulink/slref/simulink-concepts-tools.html> (accessed on 1 July 2024).
24. Hoffman, J. Modular Ku/Ka-band actively calibrated antenna tile. In Proceedings of the 2016 IEEE Aerospace Conference, Big Sky, MT, USA, 5–12 March 2016; pp. 1–6. [CrossRef]

25. Choi, K.; Liu, H. Matlab and Simulink Basics. In *Problem-Based Learning in Communication Systems Using MATLAB and Simulink*; Wiley: Hoboken, NJ, USA, 2016; pp. 1–15. [[CrossRef](#)]
26. Choi, K.; Liu, H. Quadrature Amplitude Modulation in Simulink. In *Problem-Based Learning in Communication Systems Using MATLAB and Simulink*; Wiley: Hoboken, NJ, USA, 2016; pp. 254–268. [[CrossRef](#)]

Disclaimer/Publisher’s Note: The statements, opinions and data contained in all publications are solely those of the individual author(s) and contributor(s) and not of MDPI and/or the editor(s). MDPI and/or the editor(s) disclaim responsibility for any injury to people or property resulting from any ideas, methods, instructions or products referred to in the content.